Onsite Thermal Energy Storage for Efficient and Resilient Air-conditioning in Indian Buildings

Soumyadip Bhattacharyya[1,2], Shyam Amrith[3], Pamela Fennell[3], Anurag Goyal[1*]

1: Thermal Systems Research Laboratory, Department of Mechanical Engineering, IIT Delhi, New Delhi, India;
2: Department of Civil Engineering, IIT Delhi, New Delhi, India;
3: Bartlett School Environment, Energy & Resources, University College London, London, United Kingdom

agoyal@mech.iitd.ac.in

Abstract

Thermal energy storage (TES) systems enable storing energy during off-peak hours (low demand) and release it in peak hours (high demand), improving the energy efficiency and resiliency of buildings. We present a simulation methodology to assess the performance of the TES system integrated with heating, ventilating and air-conditioning (HVAC) systems. We use a validated thermal load profile of the building in a detailed thermodynamic simulation framework to assess the feasibility of TES systems. TES coupled with HVAC systems can help improve the capabilities of building energy simulation platforms by enabling simulations of load shaving potential of TES systems and selecting the optimal material for storage. Our model can analyse the feasibility of TES for any residential or commercial building, which will help identify the most impactful categories for implementing energy storage. Our results show a load-shaving fraction of up to 38% can be achieved for a medium office building in Ahmedabad. It will help reduce the size of the vapor compression system, leading to a significant reduction in the initial capital investment and demand charges.

Keywords - thermal energy storage, building energy efficiency, load shaving, grid-interactive

1. Introduction

Rapid urbanization in India and many parts of the world will lead to a drastic increase in the demand for energy to provide comfortable residential and commercial spaces to the masses. Building energy consumption generates ~20% of the total greenhouse gas emissions. We must sustainably meet this energy demand to prevent further environmental damage while ensuring better access to clean energy and comfortable living conditions for the masses. About 50% of the total building energy consumption is due to cooling and heating (Fig. 1) [1]. Moreover, buildings cause peak demand periods that coincide with the need for cooling or heating. Peak demands strain the grid and can lead to catastrophic brownouts and blackouts. Therefore, thermal energy storage (TES) for buildings is an attractive idea to store energy in a form that can be readily used.

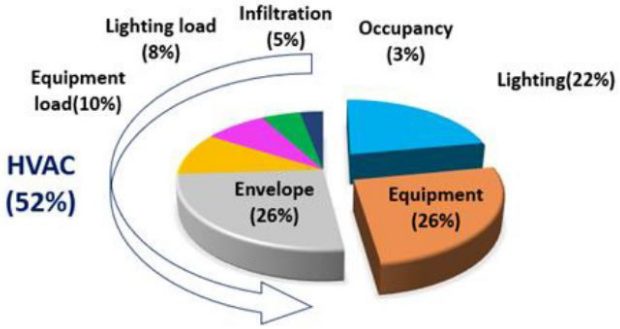

Figure 1: Components of energy consumption in buildings

Thermal energy storage (TES) systems enable storing energy during off-peak hours (low demand) and release it in peak hours (high demand), improving the energy efficiency and resiliency of buildings [2,3]. Before implementing energy storage technologies, estimating the impact on energy efficiency, resiliency, and demand response capabilities that the proposed solution can provide is essential. The available building energy simulation programs have limited capabilities to evaluate the potential of TES in buildings comprehensively [4]. The existing models have been developed using empirical models of commercial energy storage systems [5]. Therefore, the existing platforms do not allow changing the operating conditions or the storage materials. In this paper, we present a simulation methodology to assess the performance of the TES system integrated with the HVAC system. We use a validated thermal load profile of the building in a detailed thermodynamic simulation framework to assess the feasibility of TES systems. It can help improve the capabilities of building energy simulation platforms by selecting the optimum storage capacity and material.

2. Methods

2.1 System Description

We developed a detailed thermodynamic model of a vapor compression system (VCS) consisting of an air-cooled chiller coupled with a phase-change TES module based on the energy balances in each component using an overall conductance (UA) – log mean temperature difference (LMTD) method (Fig. 2). The chiller is selected to operate at a fixed cooling capacity. During the charging phase, the excess capacity of the chiller available after meeting the building cooling load is used to store energy in the TES module by freezing the material. During the discharge phase, the TES material is melted to provide balanced cooling to the building.

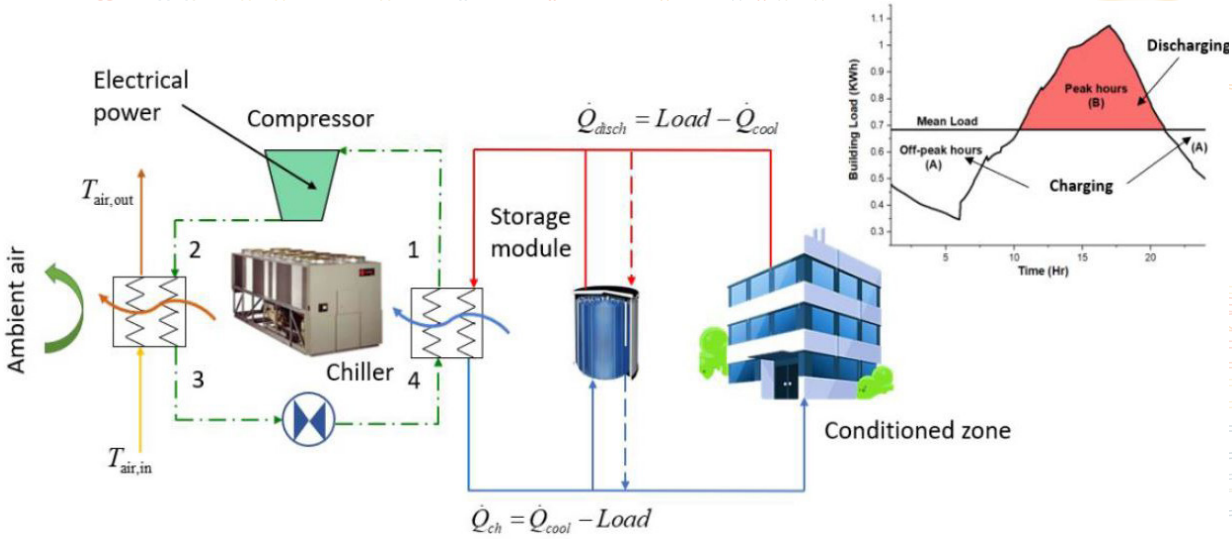

Figure 2: Schematic layout of the vapor compression cycle coupled with a TES module

2.2 Modeling Assumptions

TES is an inherently unsteady process. Therefore, for an overall system-level analysis, we simplified the dynamic heat transfer process occurring in the TES-integrated VCS by using the following assumptions:

- VCS is modeled as a quasi-steady system with all the transient effects limited to the TES module.
- Condensers and the evaporators operate under isobaric processes with negligible pressure drop.
- Storage material is always at its transition temperature, so there is no sensible heat gain or loss.
- Evaporator and condenser operate with a closest approach temperature (CAT) of 5°C.

2.3 Working Fluid and Storage Materials

We performed the analysis using R410A refrigerant in an air-cooled VCS. A propylene glycol (PG)-water mixture of 25% by weight PG is used on the evaporator coupling fluid side. We selected water/ice as the storage material with a transition temperature of 0°C and enthalpy of phase change of 336 kJ/kg. The model allows for using any phase-change material with a specified phase-change temperature and enthalpy.

2.4 Governing equations

We modeled the VCS cycle for an initial baseline condition (standard AHRI 210/240 rating condition [6]) with the above mentioned assumptions using a 10-coefficient compressor map for available compressors using Danfoss CoolSelector2® software [7]. We used Engineering Equation Solver (EES) to model the system [8]. The compressor model uses the saturated refrigerant temperature conditions in the condenser and evaporator to calculate the mass flow rate of the refrigerant and the compressor power. We selected separate compressor maps for the charging and discharging phases depending on the phase change temperature of the module and the standard cooling fluid supply conditions.

The baseline model helped determine the size (overall conductance, UA) of the condenser and evaporator for a design day. The compressor map dictates the system performance by providing the refrigerant mass flow rate and the compressor power output based on the operating conditions. Figure 2 shows the state points and components of the VCS-TES cycle. The energy balance equations for the condenser refrigerant and air stream are:

$$\dot{Q}_{cond} = \dot{m}_{ref}(h_{ref,2} - h_{ref,3}) \quad (1)$$

$$\dot{Q}_{cond} = \dot{m}_{air} C_{p,air}(T_{air,2} - T_{air,3}) \quad (2)$$

where,m_{ref} and m_{air} denote the mass flow rates of the refrigerant and the air, respectively, and href and Tair indicate the specific enthalpies of the refrigerant and air temperatures at different state points. The LMTD value is calculated across the condenser to determine the overall conductance, which is fixed for further analyses.

$$\dot{Q}_{cond} = UA_{cond} LMTD_{cond} \quad (3)$$

$$LMTD_{cond} = \frac{\Delta T_2 - \Delta T_3}{\ln \frac{\Delta T_2}{\Delta T_3}} \quad (4)$$

Here, ΔT2 and ΔT3 correspond to the temperature difference between the refrigerant and the air streams at the entry and exit of the condenser, respectively.

On the evaporator side, we calculated the volumetric flow rate of the coupling fluid (25% w/w PG-water) based on the cooling required as specified by AHRI 210/240 standard. We set the initial coupling fluid supply conditions with an approach temperature of 5°C with respect to the phase change temperature of the TES material during the charging phase. For the discharging phase, we implemented standard conditions. Using energy balance equations for the refrigerant and the coupling fluid, we calculated the overall conductance of the evaporator.

$$\dot{Q}_{eva} = \dot{m}_{ref}(h_{ref,1} - h_{ref,4}) \quad (5)$$

$$\dot{Q}_{eva} = \dot{m}_{CF} C_{p,CF}(T_{CF,1} - T_{CF,4}) \quad (6)$$

where m_{CF} denotes the mass flow rate of the coupling fluid, and TCF indicates the coupling fluid temperatures. The LMTD value is calculated across the evaporator to determine the overall conductance:

$$\dot{Q}_{eva} = UA_{eva} LMTD_{eva} \quad (7)$$

$$LMTD_{eva} = \frac{\Delta T_1 - \Delta T_4}{\ln \frac{\Delta T_1}{\Delta T_4}} \quad (8)$$

ΔT1 and ΔT4 correspond to the temperature difference between the refrigerant and the coupling fluid at the evaporator inlet and exit, respectively.

2.5 Thermal Energy Storage Module

For the TES, we formulated the charging and discharging phases based on the required cooling demand, the chiller cooling capacity, and the state of charge (SOC) of the system. The state of charge is the ratio of the quantity of storage material available at any given time to the total capacity of the module.

During the charging phase, the chiller operates at a capacity higher than required to meet the cooling demand of the building. The system performance is dictated by the outputs of the compressor map specifically designed for charging phases. We modeled the coupling fluid supply conditions from the evaporator to be at a constant temperature throughout the charging process. We considered a minimum approach temperature of 1°C for the glycol water leaving the storage module depending on the phase transition temperature of the module.
We modeled the transient heat transfer process in the TES module using a time-dependent overall conductance based on the peak charging rate, the exit setpoint temperature of the coupling fluid, and the time-varying SOC.

$$\dot{Q}_{ch,\max} = UA_{ch,\max} LMTD_{ch,design} \quad (9)$$

where $Q_{ch,max}$ denotes the peak charging rate considered for the design condition, $LMTD_{ch,design}$ corresponds to the LMTD value calculated using the coupling fluid supply and exit set point temperature and the phase transition temperature of the module, and $UA_{ch,max}$ is the maximum overall conductance of the module during charging. We calculated the actual charging rate at every time step of the simulation based on the SOC at the previous time instant and the design value of UA obtained from equation (9).

$$UA_{ch} = UA_{ch,\max} \{1 - SOC_{ch}[1 - \exp(-t_{ch} / \tau_{ch})]\} \quad (10)$$

$$\dot{Q}_{ch,actual} = UA_{ch} LMTD_{ch} \quad (11)$$

Where $Q_{ch\ actual}$, is the calculated value of the charging rate, tch is the time instant during charging, and τch is the time constant for the charging process calculated based on the total charging period. The time-dependent component of the UA function, i.e., the state of charge, denotes the increasing mass fraction of the solidified PCM in the storage module with a moving phase front. As the mass of the solid fraction increases, it offers increasing resistance to the heat extraction rate by increasing the distance of conductive heat transfer and, hence, reducing the charging rate. Assuming the storage material to remain at a constant phase-change temperature during melting or freezing, the $LMTD_{ch}$ is calculated at every time step with the PCM transition temperature as the constant high-side temperature and the coupling fluid supply and exit temperatures as the low-side temperature, respectively, as shown in the equation below.

$$LMTD_{ch} = \frac{\Delta T_{high} - \Delta T_{low}}{\ln \frac{\Delta T_{high}}{\Delta T_{low}}} \quad (12)$$

ΔT_{high} and ΔT_{low} correspond to the temperature difference between the PCM transition temperature and the coupling fluid supply temperature to the TES and the PCM transition temperature and the coupling fluid exit temperature from the TES, respectively.

The minimum value between $Q_{ch\ actual}$, and $Q_{ch\ avl}$, is considered for the charging rate in the module, where the charging rate available ($Q_{ch\ avl}$,) depends on the chiller capacity and cooling demand, and it is calculated by energy balance using the coupling fluid inlet and outlet temperatures.

$$\dot{Q}_{ch,avl} = \dot{m}_{CF} C_{p,CF} (T_{CF,out} - T_{CF,in}) \quad (13)$$

m_{CF} is the mass flow rate of the coupling fluid, $T_{CF,out}$, and $T_{CF,in}$ are the fluid exit and inlet conditions to the storage, and $C_{p,CF}$ is the specific heat of the fluid. We calculated the energy stored and the SOC of the TES as per the charging rate every time step. The SOC calculated at every time step is added to the value at the preceding time step to obtain the instantaneous SOC.

$$SOC_{ch}(t) = SOC_{ch}(t-1) + \frac{\dot{Q}_{ch,actual}(t)\Delta t_{ch}}{h_{ch} Cap} \quad (14)$$

$SOC_{ch}(t)$, $SOC_{ch}(t-1)$ are the SOC values at a given time step and its preceding instant, h_{ch} is the phase-change enthalpy of the material, and Cap is the total capacity of the storage module in terms of the mass of the material.

During the discharging phase, the chiller operates at a reduced capacity, with the storage module providing the cooling demand above the chiller capacity. We considered the return temperature of the coupling fluid to be constant throughout the discharging process. Similar to the charging process, we considered a minimum approach temperature of 1°C for the glycol-water mixture leaving the storage module.

We designed the TES module at a peak discharging rate and the exit setpoint temperature of the coupling fluid specified using the approach temperature. The overall conductance of the module is calculated using the peak discharging rate and LMTD values given below:

$$\dot{Q}_{disch,\max} = UA_{disch,\max} LMTD_{disch,design} \quad (15)$$

where $Q_{disch,max}$ denotes the peak discharging rate considered for design, $LMTD_{disch,design}$ corresponds to the LMTD value calculated using the coupling fluid supply and exit set point temperature and the phase change temperature of the module, and $UA_{disch,max}$ is the maximum overall conductance of the module during discharging. We calculated the actual discharging rate at every instant based on the SOC at the preceding time instant and the design value of UA obtained from equation (15).

$$UA_{disch} = UA_{disch,\max} SOC[\exp(-t_{disch} / \tau_{disch})] \quad (16)$$

$$\dot{Q}_{disch,actual} = UA_{disch} LMTD_{disch} \quad (17)$$

where $Q_{disch\ actual}$, is the calculated value of the discharging rate, t_{disch} is the time instant during discharging, and τ_{disch} is the time constant for the discharging process calculated based on the total discharging period. $LMTD_{disch}$ is calculated at every time step with the PCM transition temperature as the low-side temperature and the coupling fluid entry and exit temperatures as the high-side temperature, respectively, as shown in the equation below.

$$LMTD_{disch} = \frac{\Delta T_{high} - \Delta T_{low}}{\ln \frac{\Delta T_{high}}{\Delta T_{low}}} \quad (18)$$

ΔT_{high} and ΔT_{low} correspond to the temperature difference between the coupling fluid entry temperature (return from zone) and the PCM transition temperature and the coupling fluid exit temperature from the TES (supply to zone) and the PCM transition temperature, respectively.

The minimum value between $Q_{disch\ actual}$, and $Q_{disch\ req}$, is used for the discharging rate from the module at any time instant, where $Q_{disch\ req}$, is the discharging rate required to be supplied from the module depending on the chiller capacity and cooling demand, and calculated based on the energy balance using the coupling fluid entry and return temperature conditions.

$$\dot{Q}_{disch,req} = \dot{m}_{CF} C_{p,CF} (T_{CF,in} - T_{CF,out}) \quad (19)$$

where m_{CF} is the mass flow rate of the coupling fluid, $T_{CF,out}$, and $T_{CF,in}$ are the fluid exit and inlet conditions to the storage, and $C_{p,CF}$ is the specific heat of the fluid. We calculated the total discharged energy and SOC of the module using the actual discharging rate at every time instant. The SOC estimated at every time step is subtracted from the value at the preceding time step to obtain the instantaneous SOC.

$$SOC_{disch}(t) = SOC_{disch}(t-1) - \frac{\dot{Q}_{disch,actual}(t)\Delta t_{dich}}{h_{disch} Cap} \quad (20)$$

$SOC_{disch}(t)$, $SOC_{disch}(t-1)$ are the SOC values at a given time step and its preceding instant, h_{disch} is the enthalpy of phase change of the storage material, and Cap is the total capacity of the storage module measured in terms of the mass of the material.

3. Results

The model is first used to conduct design day simulations of TES-coupled HVAC systems in different climates of India [9]. The purpose of design day analysis of the TES-integrated HVAC system is to identify the extreme climatic conditions and the maximum thermal load to design and select various system components, including the compressor. It should be noted that the design day accounts for 0.4-1% of the total duration of a typical year, which means that the equipment selected under the design day operating conditions will almost always operate under relatively favorable conditions. To assess the performance in such a case, it becomes essential to study the performance and analyze the trend of different process parameters over a cooling/heating season where the temperature and the load conditions vary significantly.

We selected a medium-sized office building in Ahmedabad for a seasonal simulation with the same chiller data and compressor maps used in the design day for ice storage. We found 13 May to be the design day with the highest thermal load for a typical meteorological year. Based on that, we designed our chiller and storage module and used it to simulate the load profile for 90 days starting on 1 March. With the same thermodynamic model of storage integrated HVAC system, we incorporated a logic to reset the time steps to the initial value once a charging/discharging phase completes. We initiated our analysis on 1 March with a fully discharged TES module. We started charging it until the compressor switched from an ice-forming chiller to a standard discharge chiller, depending on the time of day and load conditions. After the end of every charging-discharging phase, the storage tank is set to charge to attain 100% SOC, following which the chiller either turns off completely or meets the building load profile. Fig. 3 shows the variation of the chiller capacities with the time-based thermal load profile for March to May. We found a peak load shaving of 38% in May(similar to the design day analysis), followed by 33% for April and 26% for March. Operating conditions in March under favorable ambient temperatures and a pattern of thermal load compared to the design day made the chiller oversized, thus reducing the peak-load shaving fraction. We also observed a reduction of 31% in peak compressor power.
Table 1 shows the utilization of the thermal storage module for all the days of a month throughout the simulation.

This result does not include the 26 weekends when the storage was fully charged and unused due to no occupancy.

Table 1: Utilization of thermal storage throughout the cooling season

TES utilization	March	April	May	Total
<10%	16	2	1	19
10-20%	3	9	3	15
20-30%	1	6	4	11
30-40%	0	2	8	10
40-50%	0	2	3	5
50-60%	0	0	1	1
60-70%	0	1	1	2
70-80%	0	0	2	2
Total (days)	**20**	**22**	**23**	**65**

To meet the building load during the off-design phases, mainly in March and early April, the system utilized up to 30% of the storage, accounting for 69% of the total duration (excluding weekends). As the weather conditions became close to the design day and the thermal loads continued to increase, storage consumption also increased.

Out of 22 working days in April, the storage capacity was utilized by up to 50% for four days, while in May, the storage was used by up to 80% for 10 days over 23 working days, equaling 43% of the total duration.

Fig 4 (left) shows the average compressor peak power variation in the three months of the cooling season for a conventional system and a system with integrated TES. As discussed above, we observed that the reduction in the compressor peak power was larger as the weather conditions and, consequently, the cooling load approached the

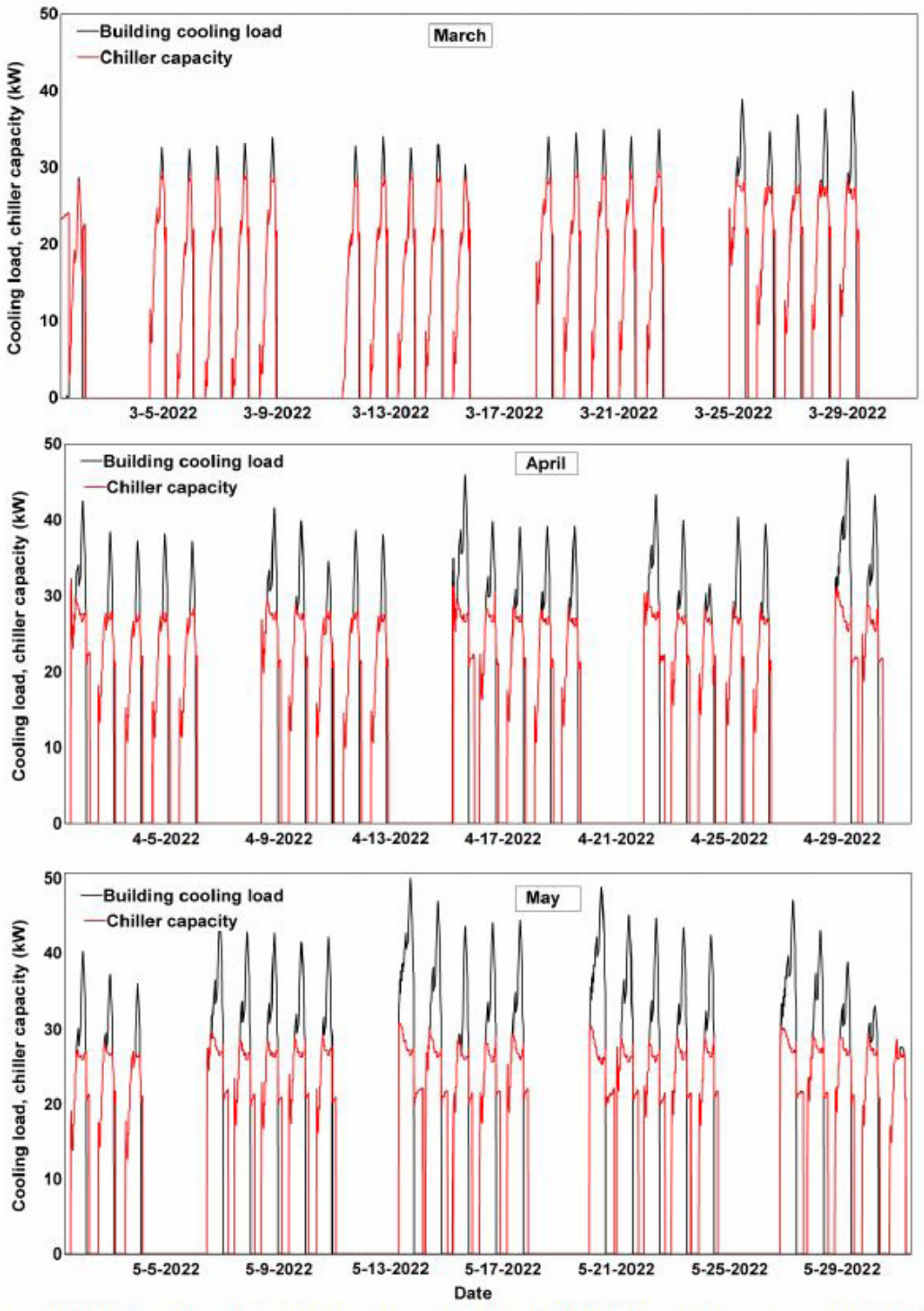

Figure 3: Variation of chiller capacity with load for the medium office building in Ahmedabad for the months of March-May

design day conditions. This is because the TES system is designed to meet the thermal load for the design day conditions. Figure 4 (right) shows the storage capacity utilization of the TES module in the cooling season. Because the TES and the compressor are designed for the maximum cooling load, the storage module capacity is not fully utilized most days. This has a significant implication on the levelized cost of storage (LCOS), which accounts for the percentage utilization of a storage asset over its lifetime. A lower utilization fraction increases the levelized cost and the cost of ownership. This is crucial to consider when designing a storage system. The costs can be significantly reduced if the storage system is sized to maximize utilization while taking a marginal penalty on peak load shaving fraction.

4. Discussion

While the proposed system could shave a significant portion of the thermal load, we also investigated the effect on the operating costs using the local electricity tariff charges (Table 2 and Fig. 5). We found that the ice storage-integrated system consumed 9075 kWh of energy, incurring a total cost of ₹44,840, while the existing system without any storage consumed 8247 kWh of energy, incurring an expenditure of ₹40,430 over three months. The excess energy was consumed to charge the storage module depending on the load profile and available state of charge after the end of the discharging phases, which, in many cases, occurred during the daytime when the ambient conditions were not favorable. The results showed that the total charging time over the entire period was 166.25 hours, with an average coefficient of performance (COP) of 2.19. The control strategy used to charge the tank leads to a low COP. Whenever the chiller switches back to the charging phase at the end of a discharging phase, it charges the tank to full capacity, regardless of weather conditions. There were instances when charging occurred at a comparatively higher ambient temperature than night conditions, yielding a low COP. We also analyzed the breakdown of the cost for each month for the office hours and the off-peak hours.investigated the effect on the operating costs using the local electricity tariff charges (Table 2 and Fig. 5). We found that the ice storage-integrated system consumed 9075 kWh of energy, incurring a total cost of ₹44,840, while the existing system without any storage consumed 8247 kWh of energy, incurring an expenditure of ₹40,430 over three months. The excess energy was consumed to charge the storage module depending on the load profile and available state of charge after charging time over the entire period was 166.25 hours, with an average coefficient of performance (COP) of 2.19. The control strategy used to charge the tank leads to a low COP. Whenever the chiller switches back to the charging phase at the end of a discharging phase, it charges the tank to full capacity, regardless of weather conditions. There were instances when charging occurred at a comparatively higher ambient temperature than night conditions, yielding a low COP. We also analyzed the breakdown of the cost for each month for the office hours and the off-peak hours.

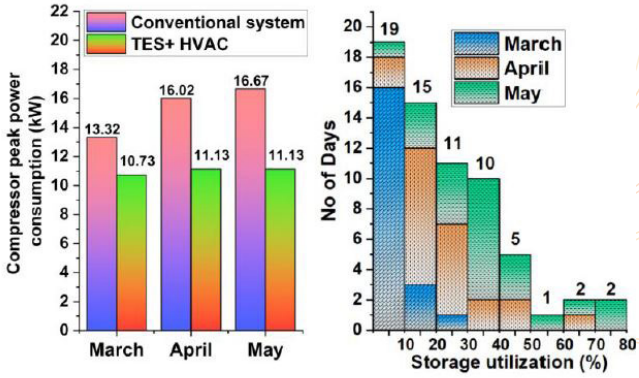

Figure 4: Variation of peak compressor power (left) for a conventional and proposed hybrid system and utilization of TES module over the three months of the cooling season (March-May) (right)

Table 2: Breakdown of operating cost based on occupancy

Time of day	March (₹)		April (₹)		May (₹)	
	Without TES	With TES	Without TES	With TES	Without TES	With TES
9 AM – 6 PM	8,318	7,937	10,809	9,654	12,366	10,489
6 PM – 9 AM	1,739	2,933	3,220	5,837	3,975	7,988
Total	10,057	10,870	14,029	15,491	16,341	18,477

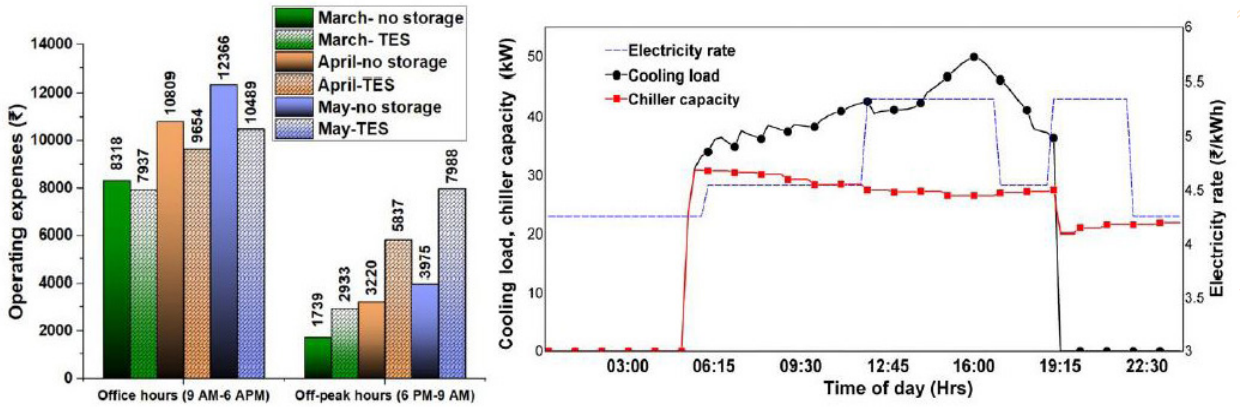

Figure 5: Variation of operating expenses during occupancy and evening hours (left) for a conventional and proposed hybrid system and a typical design day chiller capacity and load profile along with electricity tariff (right)

The tariff structure in Ahmedabad offers a base rate of ₹4.55/kWh, with a surcharge of ₹0.80/kWh during the peak period (12 PM – 5 PM, 7 PM – 10 PM), making it ₹5.35/kWh. The incentive for reduced power consumption during the off-peak period is also marginal at ₹0.30/kWh (10 PM – 6 AM) with a final off-peak rate of ₹ 4.25/kWh. Due to this unfavorable tariff structure, higher costs are incurred during the charging phase, which cannot be offset through savings obtained during the discharging phase. The techno-economic analysis of the seasonal performance of the TES-integrated system further emphasizes the revision in the electricity tariff.

5. Conclusion

This study analyzed the load-shaving potential of a phase-change TES system in a medium-sized office building in Ahmedabad for a typical cooling season. We developed a detailed thermodynamic model of a storage-integrated VCS using the first principles. While pre-defined templates based upon validated correlations are available in packaged software like EnergyPlus™, they cannot model different storage materials. It is also noteworthy that most packaged software that simulates the performance of an HVAC system use a constant COP, which is defined based on the rated capacity and the seasonal energy efficiency ratings (SEER) values, unlike our model, which calculates the COP of the system at every time instant based on the thermodynamics of the process. We simulated the performance of a TES-integrated HVAC system to determine the optimal load-shaving fraction in each case. Our analysis showed that upon integration with storage, an HVAC system could operate at a reduced capacity of ~ 38% of the rated capacity of a conventional system. The performance of the TES-integrated HVAC system showed a reduction in the compressor size by ~31%, which reduces the initial capital cost of investment. We found the existing flat tariff structure inadequate to provide significant operational cost savings, which may offset additional costs incurred for the TES system. This emphasizes implementing the time-of-day utility charges and an aggressive tariff structure to help with the broader adoption of clean energy sources.

6. Acknowledgements

The authors gratefully acknowledge the financial support from Indian Institute of Technology (IIT) Delhi and University College London (UCL) for this research project through the Multi-Institutional Faculty Interdisciplinary Research Project (MFIRP) grant - MI02475. We also appreciate discussions with Prof. Rajan Rawal and Prof. Yash Shukla from CEPT Research and Development Foundation (CRDF) in Ahmedabad, India.

5. Conclusion

This study analyzed the load-shaving potential of a phase-change TES system in a medium-sized office building in Ahmedabad for a typical cooling season. We developed a detailed thermodynamic model of a storage-integrated VCS using the first principles. While pre-defined templates based upon validated correlations are available in packaged software like EnergyPlus™, they cannot model different storage materials. It is also noteworthy that most packaged software that simulates the performance of an HVAC system use a constant COP, which is defined based on the rated capacity and the seasonal energy efficiency ratings (SEER) values, unlike our model, which calculates the COP of the system at every time instant based on the thermodynamics of the process. We simulated the performance of a TES-integrated HVAC system to determine the optimal load-shaving fraction in each case. Our analysis showed that upon integration with storage, an HVAC system could operate at a reduced capacity of ~ 38% of the rated capacity of a conventional system. The performance of the TES-integrated HVAC system showed a reduction in the compressor size by ~31%, which reduces the initial capital cost of investment. We found the existing flat tariff structure inadequate to provide significant operational cost savings, which may offset additional costs incurred for the TES system. This emphasizes implementing the time-of-day utility charges and an aggressive tariff structure to help with the broader adoption of clean energy sources.

7. References

1. Bano, F., Kamal, M. A., & Abdul, A. P. J. (2016). Examining the Role of Building Envelope for Energy Efficiency in Office Buildings in India. Architecture Research, 6(5), 107–115. https://doi.org/10.5923/j.arch.20160605.01

2. Heier, J., Bales, C., & Martin, V. (2015). Combining thermal energy storage with buildings—A review. Renewable and Sustainable Energy Reviews, 42, 1305–1325. https://doi.org/10.1016/j.rser.2014.11.031

3. Rismanchi, B., Saidur, R., Masjuki, H. H., & Mahlia, T. M. I. (2013). Modeling and simulation to determine the potential energy savings by implementing cold thermal energy storage system in office buildings. Energy Conversion and Management, 75, 152–161. https://doi.org/10.1016/j.enconman.2013.06.018

4. EnergyPlus (23.1.0). (2023). [Computer software]. U.S. Department of Energy's (DOE) Building Technologies Office (BTO). https://energyplus.net/

5. Ihm, P., Krarti, M., & Henze, G. P. (2004). Development of a thermal energy storage model for EnergyPlus. Energy and Buildings, 36(8), 807–814. https://doi.org/10.1016/j.enbuild.2004.01.021

6. AHRI Standard 210/240: Performance Rating of Unitary Air-conditioning & Air-source Heat Pump Equipment. (2017). Air Conditioning, Heating, & Refrigeration Institute (AHRI).

7. Coolselector®2. (2022). Danfoss.

8. Klein, S. A., & Alvarado, F. L. (2022). EES-Engineering Equation Solver. F-Chart Software, LLC.

9. Bhattacharyya, S., & Goyal, A. (2023). Thermal Energy Storage Systems for Enhanced Energy-efficiency and Resiliency of Commercial Buildings. Energise 2023, Goa, India, 31 October – 4 November 2023.